

**ADVANCED DETECTION OF EARLY BLIGHT (*Alternaria solani*)
DISEASE IN POTATO (*Solanum tuberosum*) PLANTS PRIOR TO VISUAL
DISEASE SYMPTOMOLOGY**

¹Daniel Atherton, ²Ruplal Choudhary, ²Dennis Watson

¹School of Agriculture, College of Business & Technology, Western Illinois University, Macomb, IL 061455

²Department of Plant, Soil and Agricultural Systems, College of Agricultural Sciences,
Southern Illinois University, Carbondale, IL 62901

ABSTRACT

Advanced detection of disease within crops can help minimize potential production losses, decrease environmental risk, and reduce the cost of farming. The objective of this study was the detection of early blight (*Alternaria solani*) in potato (*Solanum tuberosum*) plants at two different growth stages using a handheld hyperspectral spectroradiometer. Hyperspectral reflectance spectra were captured 10 times over five weeks from plants grown to the vegetative and tuber bulking growth stages. The spectra were analyzed using principal component analysis (PCA) and spectral change (ratio) analysis. PCA successfully distinguished more heavily diseased plants from healthy and minimally diseased plants using two principal components. Spectral change (ratio) analysis found optimal wavelengths (505, 510, 640, 665, 690, 750, and 935 nm) which were most sensitive to early blight infection. ANOVA results indicated a highly significant difference ($p < 0.0001$) between disease rating group means. Comparisons of diseased plants versus healthy plants using Fisher's LSD revealed more heavily diseased plants were significantly different from healthy plants. The results of this study demonstrated the capability of the PCA and spectral change (ratio) analysis techniques for detection of early blight disease in potato plants.

Keywords: Remote Sensing, Early Blight, Spectroradiometer, Potato

1.0 INTRODUCTION

Remote sensing can detect small changes in the reflectance characteristics of vegetation throughout the growing season, providing information for crop production analysis and decision making activities. Depending on the type and vigor of the vegetation, a varying amount of

energy in the visible and infrared wavelength regions is reflected by the vegetation. When vegetation suffers from one or more stress factors like drought, nutrient deficiency, and pest or disease infestation, chlorophyll production decreases, which results in a reduction of absorption in the red and blue visible regions and a subsequent increase in the amount of reflectance in these regions (Yang et al., 2010). Traditional methods for determining crop status, like pigment analysis (chlorophylls, carotenoids, and anthocyanins), are time consuming, expensive, and require destruction of the retained leaves; whereas spectral reflectance curves provide a means to ascertain pigment content with a rapid, non-invasive procedure (Gitelson et al., 2006). Empirical relationships can be established between the factors that cause plant stress and the variations observed in the resulting reflectance signatures (Jacquemoud and Ustin, 2001). Many researchers have examined vegetation pigment levels using reflectance data at specific wavelengths or by creating ratios of reflectance data values at several specific wavelengths (Gitelson et al., 2006; Gitelson et al., 2002; Blackburn, 1998a; Blackburn, 1998b; Serrano et al., 2002; Haboudane et al., 2008) or at the red-edge (Jones and Vaughan, 2010).

Spectral reflectance data provides a means for detection of disease infestation to help reduce potential production losses, restrain environmental risk, and decrease the cost of farming. Large-scale tomato growers apply pesticides, especially fungicides, on a calendar-based application schedule because the treatment window can be very short for their high-value crops (Zhang et al., 2005). An example of a fungus with a short treatment window is the fungus late blight, *Phytophthora infestans*, which has a treatment window of one week. According to Ray et al. (2011), *P. infestans* cuts global potato production by approximately 15%, but in India, one out of every three to four years, the production losses are much larger. Depending on the area and the specific weather conditions, late blight can cut yield up to 75% in major potato producing regions within India, making initial detection essential for disease control (Ray et al., 2011).

Ground field surveying has revealed that stress in wheat fields is not uniformly distributed; some areas are highly stressed while other areas are completely stress-free (Backoulou et al., 2011). According to Zhang et al. (2003), one may believe aggressive crop scouting to be the solution to aggressive diseases, but conventional ground scouting has not provided an efficient means of detection and monitoring for large tomato crops.

Irrespective of whether or not high value crops are infected with a disease, growers typically apply pesticides as insurance to diminish the risk of losing large amounts of their crop. Agricultural producers spray chemicals uniformly over entire fields to prevent or control disease, which is unnecessarily costly since disease infestation is predominately concentrated in patches around original foci where disease originates (Moshou et al., 2004), with large areas of fields free from disease at any stage of infestation (Bravo et al., 2003). In addition to higher production costs, repeated application of pesticides increases the risk of pests adapting to the pesticides,

rendering the pesticides virtually ineffective. Excessive pesticide application may also increase the amount of toxic residues contaminating ground water, making targeted pesticide placement at the correct time an important goal. To prevent overuse of chemicals, growers need a remote sensing system that can provide timely detection of diseases (Zhang et al., 2005).

Zhang et al. (2002) demonstrated the ability to distinguish healthy tomato plants from late blight infected plants using PCA, cluster analysis, and spectral ratio analysis in several fields of tomatoes with varying levels of infection. More heavily diseased plants that reached the point of economic loss could be discriminated from healthy and minimally diseased plants (Zhang et al., 2002). Zhang et al. (2003) completed supervised classification of tomato fields to distinguish late blight infected plants from healthy plants using airborne imagery. It was found that reflectance signatures for healthy plants and minimally diseased plants were highly correlated with $R^2 = 0.96$. Reflectance signatures for more severely diseased plants were also highly correlated. The correlation between reflectance signatures for healthy/minimally diseased plants and severely diseased plants was weak with $R^2 = 0.034$ (Zhang et al., 2003). Early blight, like late blight, adversely affects both tomato and potato crop yields.

Timely detection of diseases like early blight and late blight within crops is critical to minimize potential losses of production, decrease the risk of ground water contamination from over-application of pesticides, and reduce the cost of farming. Growers need advanced remote sensing research and tools to provide early detection of diseases and pests for accurate treatment.

1.1 Research Objective

This study's objective was the differentiation of healthy potato (*Solanum tuberosum*) plants from early blight (*Alternaria solani*) diseased potato plants at two growth stages using a hyperspectral spectroradiometer prior to definitive evidence of early blight disease using visual disease symptoms.

2.0 MATERIALS AND METHODS

2.1 Experimental design

The studies consisted of potato variety *Solanum tuberosum* cv. 'Canela Russet' (Holm et al., 2012) grown to the vegetative (3-6 weeks) and tuber bulking (8-12 weeks) growth stages (Pavlista, 1995). Each study consisted of a single factor, disease rating (Table 1), with repeated measures of two reflectance data capture events "measurement events" per week for 5 weeks for a total of 10 spectral data capture events. The 5-week period extended from disease inoculation to the point that the majority of inoculated plants suffered from multiple early blight blotches ("bull's eyes") on over half of the plant's foliage. A disease rating system was adapted from Zhang et al. (2002) and is detailed in Table 1 and Figure 1. Prior to each reflectance

measurement event, each plant was examined and assigned a specific disease rating. The captured reflectance values served as the independent variable.

Table 1. Disease Progression Rating Levels

Rating Level	Description
R0	Healthy plant - no indication of disease
R1	Small spots on one or two leaves of plant canopy, no "bulls eyes"
R2	Small spots on more than two leaves & less than half of plant canopy, no "bulls eyes"
R3	Small spots on more than half of plant canopy, no "bull's eyes"
R4	Single "bull's eye" (with spots) on one or two leaves of plant canopy
R5	Multiple "bull's eyes" (with spots) on more than two leaves, but less than half of plant canopy
R6	Multiple "bull's eyes" (with spots) on more than half of plant canopy

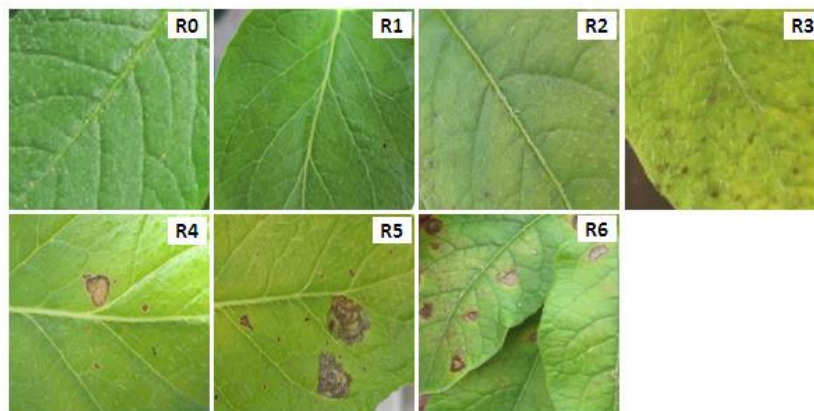


Figure 1. Disease progression by rating level

2.2 Hyperspectral reflectance equipment

An ASD FieldSpec® 3 spectroradiometer (ASD Inc., Boulder, CO) with a spectral range of 350–1,800 nm and a spectral resolution of 3 nm Full-Width-Half-Maximum (FWHM) at 700 nm and 10 nm FWHM at 1,400 nm was used to capture hyperspectral reflectance signatures from the potato plants in this study. The spectroradiometer’s sampling interval was 1.4 nm for the 350–1,000 nm range and 2 nm in the 1,000–1,800 nm range. A white reference panel that reflects nearly 100% of ambient energy was used for calibration of light source illumination, which can change as data is collected.

2.3 Potato plants and inoculation

Within a greenhouse located at the Horticulture Research Center of Southern Illinois University (Carbondale, Illinois), two similar environmental chambers were constructed to isolate the potato plants from introduction of pathogens or other outside factors. Potatoes were planted in one gallon plastic nursery pots filled 90% full with Fafard® Growing Mix 2 (Sun Gro®, Pine Bluff, AR) plant bedding material on May 10th and June 21st, 42 days apart so when inoculated with *Alternaria solani*, one set of plants were within the vegetative growth stage while a second set of plants were within the tuber bulking growth stage. The two separate plantings ensured plants within each of the two growth stages could be differentiated as healthy or infected. Each planting consisted of four replicates (Xue et al., 2004; Yao et al., 2012) of control and infected plants for a total of eight Canela Russet potato plants. All plants were watered daily. Osmocote Smart-Release® 14-14-14 (NPK) granular plant food (15 grams) was applied to each pot after planting and approximately 8 weeks thereafter. On a weekly basis, prior to inoculation with *A. solani*, each plant was randomly moved to either a new location within the same chamber or to the other chamber to minimize microclimate effects.

An equal number of vegetative and tuber bulking plants were randomly segregated into either the first or the second chamber at the time of inoculation. One chamber became the control chamber and the second chamber became the inoculation chamber. *A. solani* conidia inoculum with a concentration of 5×10^6 conidia per mL was applied to the foliage of each plant in the inoculation chamber at a rate of roughly 4 mL per plant using a spray bottle. Koch's (Schumann and D'Arcy, 2010) postulates were fulfilled while generating *A. solani* conidia for this study. A humidifier (Hydrofogger®, Hydrofogger.com, Greenville, SC) was incorporated into the inoculation chamber to provide sufficient humidity to aid in germination of the *A. solani* pathogen. Humidity was maintained near 95% for the first 48 hours after inoculation. Each day thereafter, the humidifier was operated to increase relative humidity to 90 - 95% for 6 to 8 hours during the hottest time of the day to minimize heat buildup and encourage additional spore germination, which may occur within several hours once moisture is present on foliage, then humidity was allowed to drop to the ambient humidity level for the remainder of the day.

2.4 Hyperspectral data collection

Hyperspectral reflectance signatures from each plant were captured on the day of inoculation, (just prior to inoculation) and four days thereafter and was repeated weekly for a total of 5 weeks or 10 measurement events. Measurement protocols were established to minimize environmental variability. Reflectance data was captured between 11:00 am and 1:00 pm to maximize sunlight and prior to daily watering to ensure plant moisture consistency. The spectroradiometer was allowed to run for at least 20 minutes prior to capturing reflectance data to avoid steps between wavelength regions due to different warmup rates for each sensor within the spectrometer. Each plant was centered (nadir) under the radiometer's fiber optic input, which was mounted at a

distance sufficient to achieve an instantaneous field of view (IFOV) of 80% of the plant's canopy. The IFOV contained only the plant's canopy. The spectrometer was calibrated using the white reference panel prior to capturing reflectance data from each plant. Immediately after calibration, several curves were observed to ensure reflectance varied very little from the calibrated 100% reflectance value. If reflectance varied, calibration was performed again. If reflectance did not vary, the radiometer was engaged to capture 10 hyperspectral curves from the plant over a period of 15 seconds to minimize variance from the calibrated state.

Reflectance curves were captured from the control plants, followed by the inoculated plants to reduce the risk of contaminating the control plants from prior handling of the inoculated plants. The ordering of plants within the control group and within the inoculated group was random. Plants were returned to each chamber in a different location to reduce microclimate effects. Mapping between each plant's identification tag and the captured reflectance files was logged to ensure each reflectance file could be linked to the plant responsible for the reflectance curve. The hyperspectral data was then stored for subsequent analysis.

2.5 Hyperspectral data pre-processing

The hyperspectral data curves were modified to remove wavelengths between 1355-1415 nm due to high levels of noise caused by atmospheric water vapor (ASD Inc., 2010) and between 350-400 nm due to high levels of noise (Apan et al., 2005). The hyperspectral curves were then pre-processed similar to Zhang et al. (2002) to retain reflectance values within two standard deviations of the mean for the reflectance values at each wavelength for each plant of each measurement event. Each reflectance value was compared to the mean of the other nine values at the same wavelength to determine if each value was within two standard deviations of the mean. Most of the 13,420 original reflectance values per measurement event were retained with only 0.86% of the reflectance values dropped. At each wavelength, the mean of the retained reflectance values was calculated per plant at each measurement event, like Ray et al. (2011), to obtain an initial composite signature.

Previous studies like Thenkabail et al. (2002) demonstrated bands in close proximity provide redundant information. Some researchers (Jain et al., 2007) made effective use of composite signatures averaged over 10 nm intervals. To achieve a balance between averaging at 10 nm intervals and ensuring information was not lost, the composite signatures were averaged at five nm intervals which resulted in 270 wavelengths.

2.6 Hyperspectral data analysis

2.6.1 Principal component analysis (PCA)

Analysis of the reflectance data was conducted using several complementary methods. The first

method used for analysis of the reflectance data was PCA (Zhang et al., 2002; Muhammed and Larsolle, 2003; Shahin and Symons, 2011). PCA functions as a data reduction technique by reducing a dataset to the components that hold the most value, which is the data that accounts for the majority of the variation in the dataset. The retained components provide nearly the same amount of information as the original dataset, but at a fraction of the size. The first principal component (PC) represents the largest portion of overall variation while the second PC represents the second largest portion of the overall variation and so on. In this manner, the PCs can be studied to provide insight into the differences inherent to the spectral reflectance properties of diseased and healthy plants. Determining the number of PCs to retain was essential because retaining too many components can lead to retention of unwanted noise whereas retention of too few components can lead to exclusion of crucial information. Methods used to determine an upper limit for PC retention were the scree test and eigenvalues greater than one test (SAS Institute Inc., 2008b) followed by a review of the factor loadings to determine the optimal number of factors to retain (Jensen, 2005). The principal components were computed using the PROC PRINCOMP function in SAS software (SAS Institute, 2014).

2.6.2 Spectral change (ratio) analysis

The second method used for analysis of the reflectance data was spectral change (ratio) analysis. Spectral change (ratio) curves help illuminate the disparity between the mean reflectance curve for each disease rating level and the healthy mean reflectance curve used as the reference. If the mean reflectance curve for a particular disease rating were identical to the healthy reflectance curve, the result per wavelength would be 1.0, since this would, in effect, be dividing a value by itself. If the reflectance at a particular wavelength for a diseased curve is less than the reflectance at the same wavelength for the healthy curve, the ratio will be less than 1.0. The same holds true for the inverse in which the reflectance at a particular wavelength for a diseased curve is greater than the reflectance at the same wavelength for the healthy curve, when the ratio will be greater than 1.0.

Many studies in the literature (Apan et al., 2005; Ray et al., 2011; Bravo et al., 2003; Shafri and Hamden, 2009) utilized spectra captured at one point in time so it was impossible to determine how spectral reflectance signatures changed once a plant was infected with a pathogen and the subsequent change in reflectance as the plant responded to the invading pathogen. Since this study consisted of reflectance data captured on ten different dates ranging from just prior to inoculation with *A. solani* to the later stages of the disease, changes in reflectance were analyzed to determine the extent of change in reflectance values according to the plant's disease rating level. The method used in this study to determine the extent of spectral change, similar to the method used by Zhang et al. (2002), was the division of the mean spectral reflectance curves of the diseased plants by the mean spectral reflectance curves of the healthy plants. This operation

was completed for each of the experiments. In this manner, one could determine the difference between spectral curves of plants with varying levels of disease from spectral curves of healthy plants as well as the wavelengths most sensitive to spectral change (maximum differences). Since these wavelengths provided the most value when attempting to differentiate between healthy and diseased plants, they could be considered potential optimal wavelengths for disease detection. To ascertain the statistical significance between the diseased and healthy mean spectral curves, the mean reflectance values at the optimal wavelengths were analyzed using an analysis of variance (ANOVA) with Fisher's Least Significant Difference (LSD) post-hoc multiple comparison procedure to determine if a statistically significant difference existed between mean reflectance values of diseased plants versus mean reflectance values of healthy plants. An alpha level of 0.05 was used as the level of significance for the analyses.

3.0 RESULTS

3.1 Principal Component Analysis (PCA)

PCA was completed on each experiment segregated by growth stage (vegetative (VG) or tuber bulking (TB)) for the 10 measurement events. The variance explained by each principal component (PC) along with the scree plots for each spectra can be seen in Figure 2. Eigenvector profiles can be seen in Figure 3.

The variance explained by the first, second, and remaining eigenvectors was 69.8%, 19.4%, and 10.8% for the VG stage and 66.2%, 20.7%, and 13.1% for the TB stage (fig. 2a). The scree plots exhibit an elbow at three PCs for both the VG and TB stages (fig. 2b). For each experiment, the first and second eigenvectors represented nearly 90% of the variance, so the first and second eigenvectors could be considered the PCs and the remaining eigenvectors could be dropped from the analysis. A distribution of eigenvectors is illustrated in Figure 3. The first PC for both VG and TB growth stages had greater eigenvector values in NIR while the second PC had greater eigenvector values in the visible range, demonstrating the regions with the greatest variation by PC.

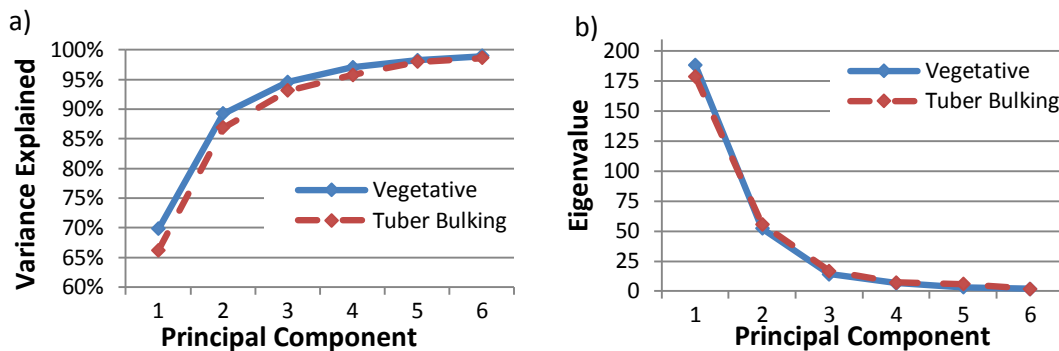


Figure 2. a) Variance explained by PC; b) Scree Plot by PC

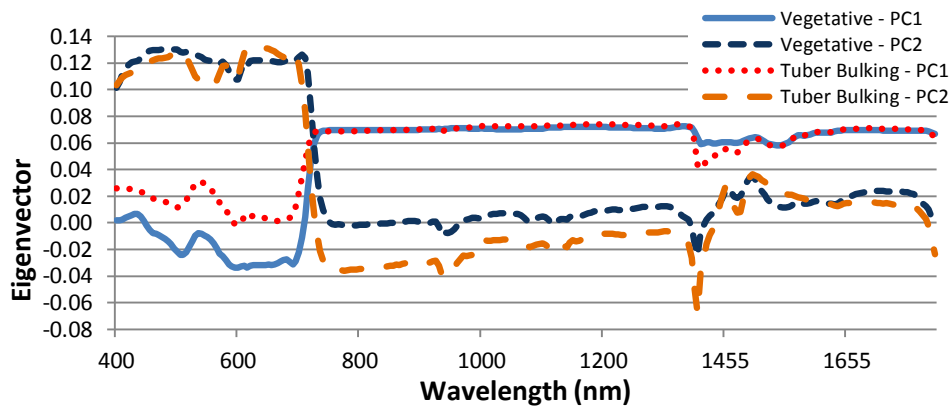


Figure 3. Eigenvector profiles for first and second eigenvectors of VG and TB stages

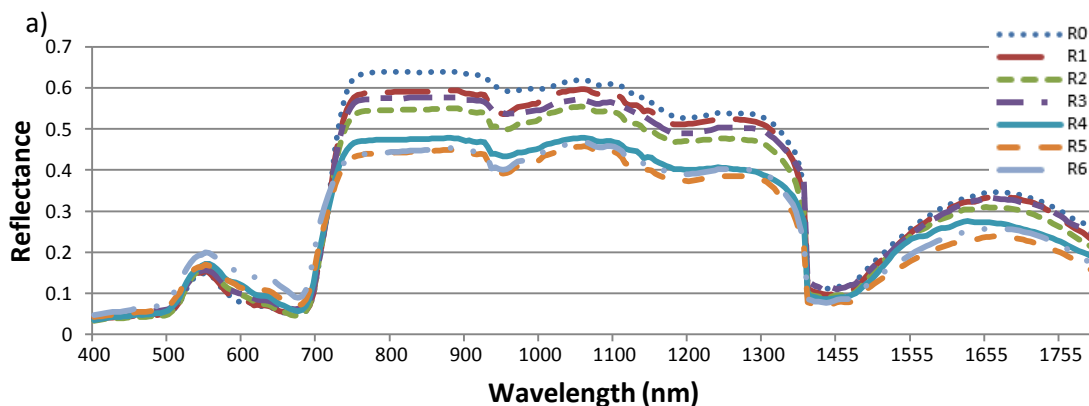
A summary of the reflectance samples with positive and negative linear correlation to the first two PCs are displayed in Table 2, similar to Zhang et al. (2002). PC1 in VG and TB stages was positively correlated with healthy (R0) and minimally infected (R1–R2) plants and negatively correlated with more heavily diseased (R4–R6) plants while PC2 was positively correlated with diseased (R5–R6) plants and negatively correlated with healthy (R0) and minimally diseased (R1–R2) plants. Since the two PCs for each experiment represented the majority of variance and were orthogonal to each other, it can be deduced that each PC represents a distinct portion of the reflectance samples. Correlation percentages may vary, but major trends in the data reveal each of the two PCs represent a different portion of the plant population.

Table 2. Correlation between spectra and PCs for plants in the VG and TB stages.

Disease Rating	Vegetative Stage				Tuber Bulking Stage			
	PC1 - Linear Correlation %		PC2 - Linear Correlation %		PC1 - Linear Correlation %		PC2 - Linear Correlation %	
	Positive	Negative	Positive	Negative	Positive	Negative	Positive	Negative
R0	68.0%	32.0%	42.0%	58.0%	60.4%	39.6%	33.3%	66.7%
R1	75.0%	25.0%	0.0%	100.0%	100.0%	0.0%	0.0%	100.0%
R2	75.0%	25.0%	25.0%	75.0%	62.5%	37.5%	25.0%	75.0%
R3	100.0%	0.0%	100.0%	0.0%	100.0%	0.0%	100.0%	0.0%
R4	11.1%	88.9%	33.3%	66.7%	20.0%	80.0%	20.0%	80.0%
R5	0.0%	100.0%	62.5%	37.5%	25.0%	75.0%	87.5%	12.5%
R6	25.0%	75.0%	100.0%	0.0%	44.4%	55.6%	88.9%	11.1%

3.2 Spectral change (ratio) analysis

Spectral change (ratio) analysis was also completed on the ten measurement events. Mean spectral curves segregated by disease rating are depicted in Figure 4. Spectral ratios were calculated by dividing each mean diseased spectral reflectance curve by the mean healthy spectral reflectance curve at each wavelength for each experiment. The ratios of mean diseased reflectance curve by disease rating level to the mean healthy reflectance curve are illustrated in Figure 5. Wavelengths of interest between 400-1,000 nm were identified; higher wavelengths were removed from the figure for clarity.



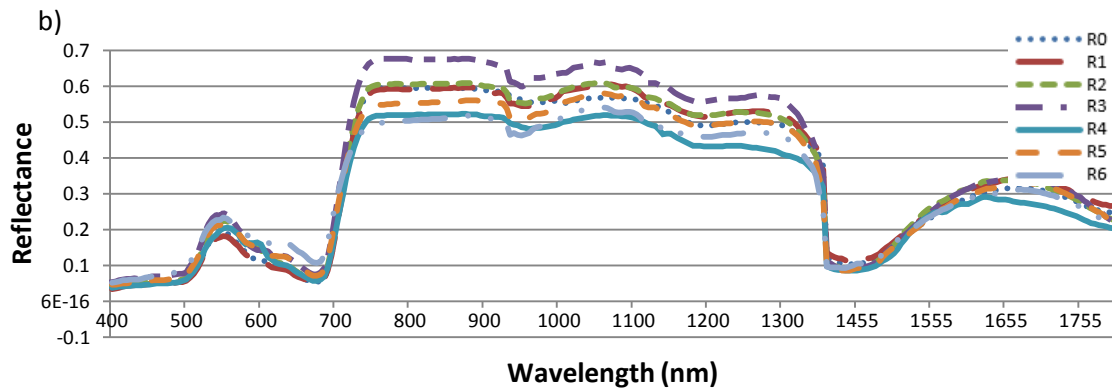
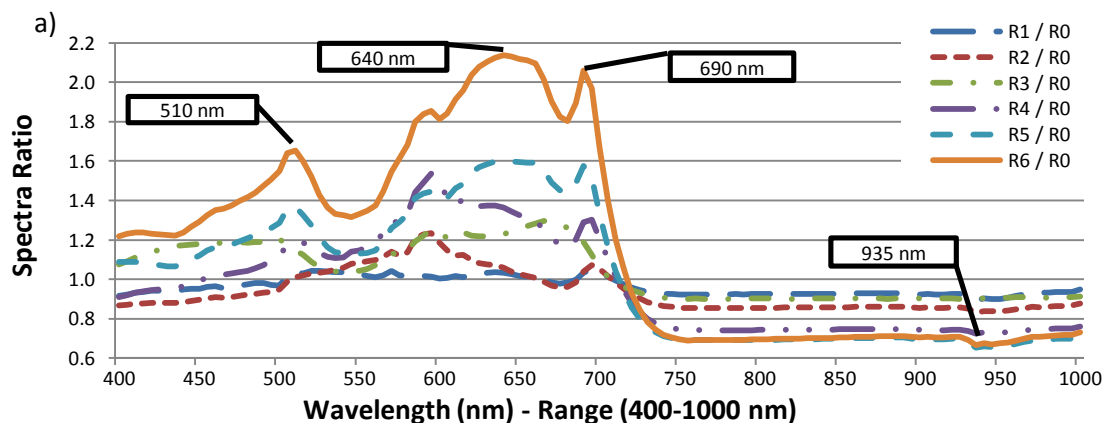


Figure 4. Mean spectra of plants in a) VG stage; b) TB stage. Note: n = sample size.

The wavelengths that appear most sensitive or provide the greatest amount of change for the various ratios were found at 510, 640, 690, and 935 nm for VG (fig. 5a) and 505, 665, 750, and 935 nm for TB (fig. 5b). From 1,000–1,800 nm, two regions (near 1,355 nm and near 1,800 nm) demonstrated increased sensitivity compared to other wavelengths within that range. Atmospheric water vapor may absorb light energy near 1400 nm and 1800 nm resulting in inconsistent reflectance levels from vegetation (ASD Inc., 2010). Since the wavelengths near 1355 nm and 1800 nm may be suspect due to their proximity to known areas of atmospheric water vapor variation, these wavelengths were excluded from the potential optimal wavelengths. The proposed optimal wavelengths for this study were found to be 505, 510, 640, 665, 690, 750, and 935 nm.



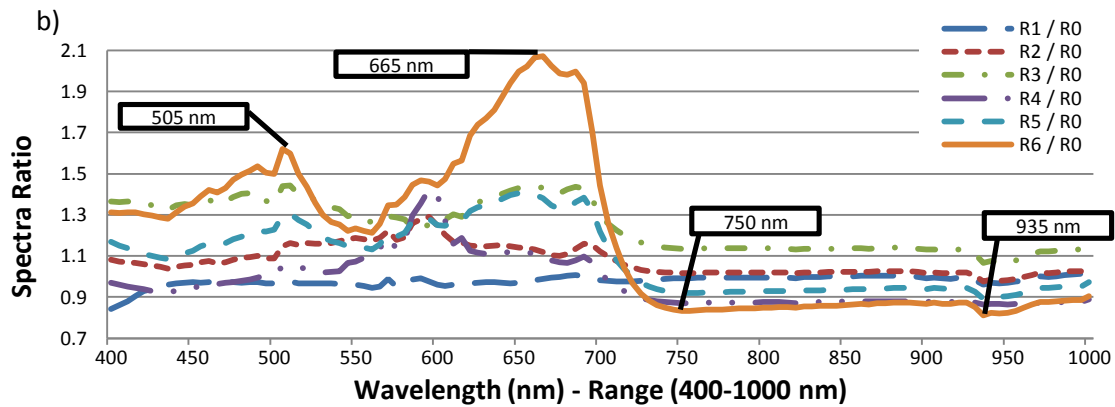


Figure 5. Ratios of diseased to healthy plants in a) VG stage; b) TB stage.

Spectra consisting of reflectance values at the proposed optimal wavelengths were then used to complete an Analysis of Variance (ANOVA) followed by Fisher’s LSD multiple comparison procedure (MCP). Omnibus ANOVA results were $F_{(27, 132)} = 128.92, p < 0.0001$ and $F_{(27, 132)} = 100.82, p < 0.0001$, respectively for the VG stage and the TB stage indicating a highly significant difference between disease rating group means. Fisher’s LSD, in Table 3, demonstrated significant differences between diseased (R2, R4, and R5) plants and healthy (R0) plants for the VG stage and diseased (R4) plants and healthy (R0) plants for the tuber bulking stage. Sample size was not identical across the disease rating levels due to differences in the speed of disease progression.

Table 3. Fisher’s LSD using proposed optimal wavelengths.

Vegetative Stage				Tuber Bulking Stage			
Rating	N	Mean	Std Dev	Rating	N	Mean	Std Dev
R0	10	0.201	0.026	R0	8	0.322	0.028
R1	4	0.187	0.025	R1	1	0.314	
R2	4	0.178*	0.039	R2	8	0.325	0.039
R3	1	0.196		R3	1	0.365	
R4	9	0.173*	0.033	R4	5	0.285*	0.058
R5	8	0.174*	0.021	R5	8	0.305	0.041
R6	4	0.198	0.037	R6	9	0.295	0.063

* Significant at 0.05 level

4.0 DISCUSSION

Timely detection of insect and disease infestation within crops is critical to minimize potential losses of production, decrease the risk of ground water contamination from over-application of pesticides, and reduce the cost of farming. This study used several complementary methods to demonstrate the possibility of using spectral reflectance data to differentiate infected plants from healthy plants.

Principal component analysis (PCA) found PC1 and PC2 were able to differentiate more heavily diseased (R5–R6) plants from healthy and minimally diseased (R1–R2) plants, since each PC represented a different segment of the plant population (Table 4). The principal sources of variation were healthy (R0) and minimally diseased (R1–R2) plants (PC1), followed by more heavily diseased (R5–R6) plants (PC2). R3 and R4 disease ratings were inconclusive. These results were similar to results found by Zhang et al. (2002) using PCA on reflectance spectra from late blight infected tomato plants, in which more heavily infected plants could readily be differentiated from healthy and minimally diseased plants using two PCs.

Table 4. Groups of plant population represented by principal components.

Principal Component Segment Representation		
Growth Stage	PC 1	PC 2
Vegetative	Healthy (R0) & Minimally Diseased (R1 – R2)	Diseased (R5 – R6)
Tuber Bulking	Healthy (R0) & Minimally Diseased (R1 – R2)	Diseased (R5 – R6)

Analysis of the reflectance spectra using spectral change (ratio) analysis revealed a significant difference between diseased plants and healthy plants to varying degrees depending upon the growth stage (Table 3). Comparing results of Table 3 to the results in Table 2 (PCA), one can see a direct correlation between the disease rating levels included in PC1 versus PC2. This shows spectral change analysis is capable of differentiating more heavily diseased (R5–R6) plants from healthy (R0) and minimally diseased (R1–R2) plants.

The proposed optimal wavelength regions found for detection of early blight in this study (505–510, 640, 665, 690, 750, and 935 nm) were similar to optimal wavelengths (543, 663, 761, and 1993 nm) found by Zhang et al. (2002) while completing spectral change analysis on tomatoes infected with late blight. In the visible spectrum (roughly 400-700 nm), the leaf pigments chlorophyll a, chlorophyll b, and carotenes absorb much of the energy reaching the vegetation in the blue (450 nm) and red ranges (680 nm) (Jensen, 2005). Many of the wavelengths were within the “blue” and “red” visible wavelength regions that correspond to areas of high energy

absorption by chlorophyll, which is adversely affected when a plant is infected with a disease (Gitelson et al., 2001). Another photosynthetic pigment, anthocyanin (red pigments), aids in photosynthesis and protects leaves from excess light energy (Gitelson et al., 2006). Accumulation of anthocyanins result from drought, nutrient deficiencies, and bacterial and fungal infections (Gitelson et al., 2001). When a plant suffers from a stress factor such as pest or disease infestation, normal chlorophyll production diminishes, followed by a decrease in absorption and an increase in reflectance in the blue and red visible regions (Yang et al., 2010). Wavelengths within the NIR region also reduce reflectance because as the mesophyll layer of the plants leaves responds to pathogen invasion, the reflective capacity of the mesophyll layer decreases, causing a reduction in the NIR energy reflected.

In this study, differentiation of diseased plants (R5-R6) from healthy plants (R0) was possible because the chlorophyll, carotene, and anthocyanin content had deteriorated to an extent that a statistically significant difference existed between the reflectance signatures of the more heavily diseased plants and the healthy plants. The ability to discern healthy (R0) plants from minimally diseased (R1–R2) plants would clearly be optimal, but the differentiation of minimally diseased plants (R1-R2) from healthy plants was not possible because even though the chlorophyll, carotene, and anthocyanin content of the minimally diseased plants had deteriorated from that of the healthy plants, the deterioration was not to the extent that a statistically significant difference existed between the reflectance signatures of the minimally diseased plants and the healthy plants.

5.0 CONCLUSIONS

Hyperspectral reflectance spectra captured twice weekly for five weeks from Canela Russet potato plants grown to the vegetative (3–6 weeks) and tuber bulking (8–12 weeks) growth stages were analyzed using principal component analysis (PCA) and spectral change (ratio) analysis to determine if early blight could be detected. PCA demonstrated the capability of successfully distinguishing more heavily diseased plants from healthy and minimally diseased plants using two principal components.

Spectral change (ratio) analysis provided wavelengths (505, 510, 640, 665, 690, 750, and 935 nm) most sensitive to early blight. ANOVA results indicated a highly significant difference ($p < 0.0001$) between disease rating group means. In the majority of the experiments, comparisons of diseased (R1–R6) plants with healthy (R0) plants using Fisher's LSD revealed more heavily diseased plants were significantly different from healthy plants.

The plants used for this study were grown in closed chambers and reflectance data was captured in a greenhouse environment. Additional research should be conducted to substantiate the results obtained in this study and to determine whether these results differ from field based results.

REFERENCES

- Apan, A., B. Datt, and R. Kelly. (2005). Detection of Pests and Disease in Vegetable Crops Using Hyperspectral Sensing: A Comparison of Data for Different Symptoms. *Proceedings of SSC 2005 Spatial Intelligence and Innovation*, 10-18.
- ASD, Inc. (2010). Field Spec 3 User Manual. Boulder, CO, USA.
- Backoulou, G., N. Elliott, K. Giles, M. Phoofolo, and V. Catana. (2011). Development of a method using multispectral imagery and spatial pattern metrics to quantify stress to wheat fields caused by *Diuraphis noxia*. *Computers and Electronics in Agriculture*, 75, 64-70.
- Blackburn, G. (1998a). Spectral indices for estimating photosynthetic pigment concentrations: a test using senescent tree leaves. *International Journal of Remote Sensing*, 4, 657-675.
- Blackburn, G. (1998b). Quantifying Chlorophylls and Carotenoids at Leaf and Canopy Scales: An Evaluation of Some Hyperspectral Approaches. *Remote Sensing of the Environment*, 66, 273-285.
- Bravo, C., D. Moshou, J. West, A. McCartney, and H. Ramon. (2003). Early Disease Detection in Wheat Fields using Spectral Reflectance. *Biosystems Engineering*, 2, 137-145.
- Gitelson, A., G. Keydan, and M. Merzlyak. (2006). Three-band model for noninvasive estimation of chlorophyll, carotenoids, and anthocyanin contents in higher plant leaves. *Geophysical Research Letters*, 33, 1-5.
- Gitelson, A., M. Merzlyak, and O. Chivkunova. (2001). Optical Properties and Nondestructive Estimation of Anthocyanin Content in Plant Leaves. *Photochemistry and Photobiology*, 1, 38-45.
- Gitelson, A., Y. Zur, O. Chivkunova, and M. Merzlyak. (2002). Assessing Carotenoid Content in Plant Leaves with Reflectance. *Photochemistry and Photobiology*, 3, 272-281.
- Haboudane, D., N. Tremblay, J. Miller, and P. Vigneault. (2008). Remote Estimation of Crop Chlorophyll Content Using Spectral Indices Derived From Hyperspectral Data. *IEEE Transactions on Geoscience and Remote Sensing*, 2, 423-437.
- Holm, D., S. Essah, and R. Davidson. (2012). Canela Russet Information Sheet . Fort Collins : Colorado State University.
- Jacquemoud, S. and S. Ustin. (2001). Leaf Optical Properties: A State of the Art. 8th International Symposium of Physical Measurements & Signatures in Remote Sensing, CNES, 223-232.
- Jain, N., S. Ray, J. Singh, and S. Panigrahy. (2007). Use of hyperspectral data to assess the effects of different nitrogen applications on a potato crop. *Precision Agriculture*, 225-239.

Jensen, J. R. (2005). *Introductory Digital Image Processing: Remote Sensing*. Upper Saddle River: Pearson Prentice Hall.

Jones, H. and R. Vaughan. (2010). *Remote Sensing of Vegetation* (1st ed.). Oxford: Oxford University Press.

Moshou, D., C. Bravo, J. West, S. Wahlen, A. McCartney, and H. Ramon. (2004). Automatic detection of 'yellow rust' in wheat using reflectance measurements and neural networks. *Computers and Electronics in Agriculture*, 44, 173-188.

Muhammed, H., & Larsolle, A. (2003). Feature Vector Based Analysis of Hyperspectral Crop Reflectance Data for Discrimination and Quantification of Fungal Disease Severity in Wheat. *Biosystems Engineering*, 86, 125-134.

Pavlista, A. (1995). EC95-1249 Potato Production Stages: Scheduling Key Practices. Lincoln: Historical Materials from University of Nebraska-Lincoln Extension.

Ray, S., N. Jain, R. Aoroa, S. Chavan, and S. Panigrahy. (2011). Utility of Hyperspectral Data for Potato Late Blight Disease Detection. *Journal of Indian Society of Remote Sensing*, 2, 337-354.

SAS Institute. (2014). *SAS User's Guide*. Version 9.3. Cary, NC, U.S.A.

SAS Institute Inc. (2008b). *SAS/STAT® 9.2 User's Guide [The PRINCOMP Procedure]*. Cary, NC: SAS Institute Inc.

Schumann, G., & D'Arcy, C. (2010). *Essential Plant Pathology*. St. Paul: The American Phytopathological Society.

Serrano, L., J. Penuelas, and S. Ustin. (2002). Remote sensing of nitrogen and lignin in Mediterranean vegetation from AVIRIS data: Decomposing biochemical from structural signals. *Remote Sensing of the Environment*, 81, 355-364.

Shafri, H. and N. Hamden. (2009). Hyperspectral Imagery for Mapping Disease Infection in Oil Palm Plantation Using Vegetation Indices and Red Edge Technique. *American Journal of Applied Sciences*, 6, 1031-1035.

Shahin, M. and S. Symons. (2011). Detection of Fusarium damaged kernels in Canada Western Red Spring wheat using hyperspectral imaging and principal component analysis. *Computers and Electronics in Agriculture*, 75, 107-112.

Thenkabail, P., R. Smith, and E. De Pauw. (2002). Evaluation of Narrowband and Broadband Vegetation Indices for Determining Wavebands for Crop Characterization. *Photogrammetric Engineering & Remote Sensing*, 6, 607-621.

Xue, L., W. Cao, W. Luo, T. Dai, and Y. Zhu. (2004). Monitoring Lead Nitrogen Status in Rice with Canopy Spectral Reflectance. *Agronomy Journal*, 96, 135-142.

Yang, F., J. Li, X. Gan, Y. Qian, X. Wu, and Q. Yang. (2010). Assessing nutritional status of *Festuca arundinacea* by monitoring photosynthetic pigments from hyperspectral data. *Computers and Electronics in Agriculture*, 70, 52-59.

Yao, H., Y. Huang, Z. Hruska, S. Thomson, and K. Reddy. (2012). Using Vegetation Index and Modified Derivative for Early Detection of Soybean Injury from Glyphosate. *Computers and Electronics in Agriculture*, 145-157.

Zhang, M., X. Liu, and M. O'Neill. (2002). Spectral discrimination of *Phytophthora infestans* infection on tomatoes based on principal component and cluster analyses. *International Journal of Remote Sensing*, 23, 1095-1107.

Zhang, M., Z. Qin, and X. Liu. (2005). Remote Spectral Imagery to Detect Late Blight in Tomatoes. *Precision Agriculture* 6, 489-508.

Zhang, M., Z. Qin, X. Liu, and S. Ustin. (2003). Detection of stress in tomatoes induced by late blight disease in California, using hyperspectral remote sensing. *International Journal of Applied Earth Observation and Geoinformation*, 295-310.